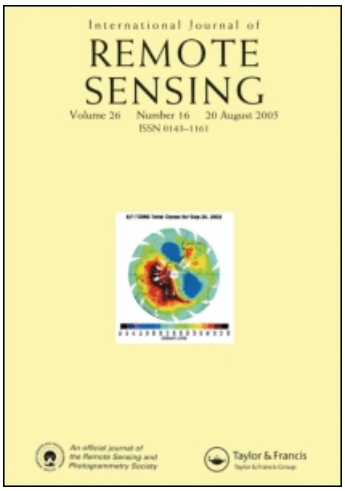

International Journal of Remote Sensing
Publication details, including instructions for authors and subscription information:
http://www.informaworld.com/smpp/title~content=t713722504

Operational land cover change detection using change vector analysis

C. C. Kontoes [a]
[a] Institute for Space Applications and Remote Sensing, National Observatory of Athens, GR 15236 Athens, Greece

First Published:2008

To cite this Article Kontoes, C. C.(2008)'Operational land cover change detection using change vector analysis',International Journal of Remote Sensing,29:16,4757 — 4779
To link to this Article: DOI: 10.1080/01431160801961367
URL: http://dx.doi.org/10.1080/01431160801961367

International Journal of Remote Sensing
Vol. 29, No. 16, 20 August 2008, 4757–4779

Taylor & Francis
Taylor & Francis Group

Operational land cover change detection using change vector analysis

C. C. KONTOES*
Institute for Space Applications and Remote Sensing, National Observatory of Athens, Metaxa and Vas. Pavlou Str., GR 15236 Athens, Greece

(*Received 15 October 2005; in final form 5 February 2008*)

This research study introduces the use of a change detection and classification algorithm that relies on the change vector analysis (CVA) method. Its implementation aims to ensure adequate response to operational production needs and allow optimized data processing over extended and environmentally complex areas. Automatic change class labelling relies on the use of a $(3n+2)$-dimensional feature space, where n denotes the number of sensor bands. Such enhanced feature space allows for a finer and more accurate definition of change classes of the 'from-to' type. Moreover, and to efficiently address the problem of change area overestimation, the proposed method takes into account specific evidence derived from the pixel's geographic neighbourhood, the latter defined as a 3×3 pixel kernel. The performance of this integrated algorithmic approach has been tested and validated in the framework of the CORINE Land Cover-Greece 2000 and the ESA/GSE Forest Monitoring projects in three test sites located in the outskirts of the city of Ptolemais, Thasos island and the suburbs of Athens in Greece. Its implementation in such highly fragmented and dynamically changing landscape environments has resulted in qualified and accurate land cover change maps, achieving an overall level of classification accuracy of 88–96%. Compared to visual image interpretation, the method requires half the effort. In conclusion, the proposed method has proved effective and can be recommended for use in the framework of operational projects.

1. Introduction

Change detection is an increasingly popular remote sensing application. It concerns the process of identifying differences in the state of an object or phenomenon by observing it at different times (Singh 1989, Nelson 1983). This is essential for understanding natural and artificial processes (e.g. land–atmosphere interactions and energy flows, biological productivity, spread of disturbances) that influence the ecological balance at local, regional and global levels (Avissar and Pielke 1989, Henderson-Sellers and Pitman 1992, William *et al.* 1994).

The major aspects of a change detection study involve mapping and identifying the nature of the changes. Multitemporal satellite image acquisitions have been used in several studies for land surface change mapping and labelling (Coppin and Bauer 1996, Jensen 1996, Ding *et al.* 1998, Johnson and Kasischke 1998, Chen *et al.* 2003). The commonly used approach compares a minimum of two satellite images acquired in early and late stages of the period under study. Such satellite images are classified and the resulting classification layers are compared with each other to identify classes of

*Email: kontoes@space.noa.gr

International Journal of Remote Sensing
ISSN 0143-1161 print/ISSN 1366-5901 online
http://www.tandf.co.uk/journals
DOI: 10.1080/01431160801961367

land cover changes. Other studies make direct use of pixel brightness. Specific band transformations and band operations are used for depicting the areas and types of change that may have arisen (Weismiller *et al.* 1977, Howarth and Wickware 1981, Fung and Ledrew 1988, Pilon *et al.* 1988, Macleod and Congalton 1998). The pixel brightness is transformed to information layers directly related to land cover and land cover change conditions. Such information layers have been representative forms of vegetation indices because they are highly correlated to crown closure, leaf area index and vegetation parameters (Tucker 1979, Running *et al.* 1986, Singh 1986). In practice, seasonal and/or permanent changes in vegetation cover are mapped by analysing the magnitude of change of the vegetation indices under study (Marsh *et al.* 1992, Tappan *et al.* 1992, Lyon *et al.* 1998). In a similar approach, a principal component transformation is applied on a multidate image vector (Fung and Ledrew 1987, Eastman and Fulk 1993, Hayes and Sader 2001). Reported advantages of this approach include improved interpretability, isolation of seasonal effects, better statistical control and more precise classifications. In this approach the first two components tend to represent variations that are associated with seasonal land cover instability and overall image noise (e.g. due to atmospheric disturbances), while higher order components represent actual changes in the landscape.

Several studies (Engvall *et al.* 1977, Malila 1980, Lambin and Strahler 1994, Sohl 1999, Chen *et al.* 2003) have made use of the so-called change vectors, defined as the radiometric vector difference between the two-date satellite image acquisitions. In these studies the magnitude of the change vector and its direction cosines are used to interpret the recorded land cover changes in the area of interest. This method is reported in the literature as change vector analysis (CVA).

The CVA method makes direct use of the image radiometric information and returns classifications of the 'from-to' type for the change classes. The method identifies gradual modifications of land cover types. However, depending on the area complexity and rate of change dynamics, the labelling process may face limitations if it is solely based on the use of the change vector magnitude and direction cosines.

This paper proposes the use of the CVA method in an operational production environment. The proposed method allows for optimized data processing over extended and environmentally complex areas. Minimal data preprocessing is ensured through the use of common image radiometric and image registration techniques. Furthermore, a specific algorithm for delineating 'change/no-change' areas has been developed and tested. The algorithm analyses the spatial context of the pixel defined as a 3×3 pixel kernel.

The proposed change classification algorithm also makes use of a $(3n+2)$-dimensional feature space, where n denotes the number of sensor bands. This enhanced feature space enables a finer and more accurate definition of the existing change classes. The algorithm performance has been tested and validated in the framework of two operational change detection projects, the CORINE Land Cover-Greece 2000 project and the ESA/GSE Forest Monitoring project. A detailed overview of the change classification analysis conducted in this research study is presented in section 4, together with the corresponding classification accuracy results.

2. Meeting the operational mapping requirement

Territorial mapping of land use/land cover changes has been recognized as an essential parameter in integrated environmental assessment. To this end, the

European Environment Agency (EEA), the European Commission (EC) and the European Space Agency (ESA) have initiated operational mapping programmes such as the CORINE Land Cover 2000 (CLC2000), the CORINE Land Cover Change (CLC-Change) and the Global Monitoring for Environment and Security (GMES). In this context two operational projects were implemented in Greece: (1) the CLC2000-Greece project and (2) the Forest Monitoring GMES/GSE/ESA project. These projects involved the use of visual image interpretation of multidate image acquisitions in combination with pixel-based classifications to generate land cover and land cover change information over Greece. Classification accuracy and mapping precision have been identified as crucial parameters in both projects. Product compliance with the specified standards was ensured by specific validation and quality assessment procedures. This required intense effort dedicated to visual image interpretation and *in situ* data collection and, as a result, project costs were considerably increased. In such an operational context the proposed CVA method has proved to be an efficient and less expensive solution as demonstrated below.

3. Methodological approach

3.1 *The feature space*

A change vector can be described as an angle of change (direction of the change vector) plus a magnitude of change (size of the change vector) between the reference date and the current date (Jensen *et al.* 1996), denoted here as Date 1 and Date 2, respectively. Obviously the greater the magnitude of change vector $\overrightarrow{\Delta G}$, the higher the probability of change occurrence between the two dates.

Two images of n bands, acquired on Dates 1 and 2, respectively, are represented as vectors in the n-dimensional image space. Let the image of Date 1 be denoted as vector $\overrightarrow{G_1} = (g_{11}, g_{12}, \ldots, g_{1n})^T$ and the image of Date 2 as vector $\overrightarrow{G_2} = (g_{21}, g_{22}, \ldots, g_{2n})^T$. Change vector $\overrightarrow{\Delta G}$ is then defined as:

$$\overrightarrow{\Delta G} = \begin{pmatrix} g_{11} - g_{21} \\ g_{12} - g_{22} \\ \cdots \\ g_{1n} - g_{2n} \end{pmatrix} = \begin{pmatrix} \delta g_1 \\ \delta g_2 \\ \cdots \\ \delta g_n \end{pmatrix} \tag{1}$$

and the magnitude of change vector $\overrightarrow{\Delta G}$ as:

$$\left|\overrightarrow{\Delta G}\right| = \sqrt{\delta g_1^2 + \delta g_2^2 + \ldots + \delta g_n^2} \tag{2}$$

The direction of change in the n-dimensional image space is represented by the cosine functions of direction angles $c_1, c_2, \ldots, c_n$ of the change vector $\overrightarrow{\Delta G}$. The direction angles are thus defined as:

$$c_1 = \arccos \frac{\delta g_1}{\left|\overrightarrow{\Delta G}\right|}, \; c_2 = \arccos \frac{\delta g_2}{\left|\overrightarrow{\Delta G}\right|}, \; \ldots, \; c_n = \arccos \frac{\delta g_n}{\left|\overrightarrow{\Delta G}\right|} \tag{3}$$

The direction of change can be represented as one point in the direction cosine or direction angle spaces, defined by vectors $\overrightarrow{Z} = (\cos c_1, \cos c_2, \ldots, \cos c_n)$ and $\overrightarrow{Z} = (c_1, c_2, \ldots, c_n)$, respectively.

According to the CVA method, the calculated magnitude of change and the direction of change are used as a means to identify classes of land cover changes.

This can, in practice, be achieved by classifying the cloud of points $\overrightarrow{Z}=(c_1, c_2, \ldots, c_n)$ in the direction cosine or direction angle feature spaces (Chen *et al.* 2003).

However, the combined use of the magnitude of change and the direction of change does not represent the reported land cover change types in a unique way. As illustrated in figure 1(*b*), many different pairs of vectors $\overrightarrow{G_1}$ and $\overrightarrow{G_2}$ exist and this may result in the same change vector $\overrightarrow{\Delta G}$ (same size and direction) or a very similar one as far as clustering is concerned. It is therefore necessary to integrate additional information in the data clustering process. As a way to overcome this problem, Chen *et al.* (2003) suggested a supervised approach that makes use of training pixels representative to land cover classes recorded on the Date 1 image. The spectral differences between any pair of training pixels are calculated in order to define a representative set of change vectors that are then transplanted into the direction cosine space. The training pixels together with the representative change vectors are used as signatures for image classification and 'from-to' class labelling. Obviously, to efficiently address the change classification problem with this method, all class members of the 'from-to' type classes should be exhaustively represented on the Date 1 image, which is used for seed pixel selection and classification training.

In light of these remarks and to enhance the implementation efficiency in the framework of operational projects, an unsupervised change clustering approach is proposed and analytically presented in this research study. An advantage of this method, as opposed to previous supervised ones, is the absence of any effort required to identify adequate training data for change types. The unsupervised approach, however, requires the definition of a proper feature space to ensure finer definitions of non-overlapping change clusters. The definition process of the proposed feature space is presented below. For simplicity purposes, a three-dimensional image space has been used in the analysis.

Let us consider feature space $\overrightarrow{Z}$, which is composed of the magnitude and the direction of change vector $\overrightarrow{\Delta G}$ (figure 1(*b*)). As noted above, in the general case a 'one to many' relation ($1 \rightarrow n$) exists between measurement vector $\overrightarrow{Z}$ for a pixel and the change types it may represent (figure 1(*b*)). Therefore, to divide the radiometric image space into finer sections and obtain well-defined change clusters, the integration of additional information into the feature space and thus the creation of an enhanced feature space $\overrightarrow{Z}$ is required. This is further explained in the following paragraphs.

Let us consider that measurement vector $\overrightarrow{Z}$ is modified by introducing four new elements, namely the magnitude $\left|\overrightarrow{G_1}\right|$ and cosine functions of direction angles θ_{XG1}, θ_{YG1} and θ_{ZG1} of vector $\overrightarrow{G_1}=(g_{11}, g_{12}, g_{13})^T$. The insertion of vector $\overrightarrow{G_1}$ in $\overrightarrow{Z}$ imposes an important restriction on the clustering process. It substantially reduces confusion in clustering and enhances the relation between measurement vector $\overrightarrow{Z}$ for a pixel and the number of change classes it can represent. Indeed, the number of possible solutions is now drawn from two distinct clusters, represented by the two equal in magnitude and opposite in sign change vectors $\overrightarrow{\Delta G_1}$ and $\overrightarrow{\Delta G_2}$ illustrated in figure 1(*c*). This is possible because the opposite sign vectors have the same magnitude $\left|\overrightarrow{\Delta G}\right|$ and the same direction cosine functions. To further reduce the set of possible solutions and focus on a single change cluster, it is necessary that a new set of feature parameters is defined and added to the feature space $\overrightarrow{Z}$.

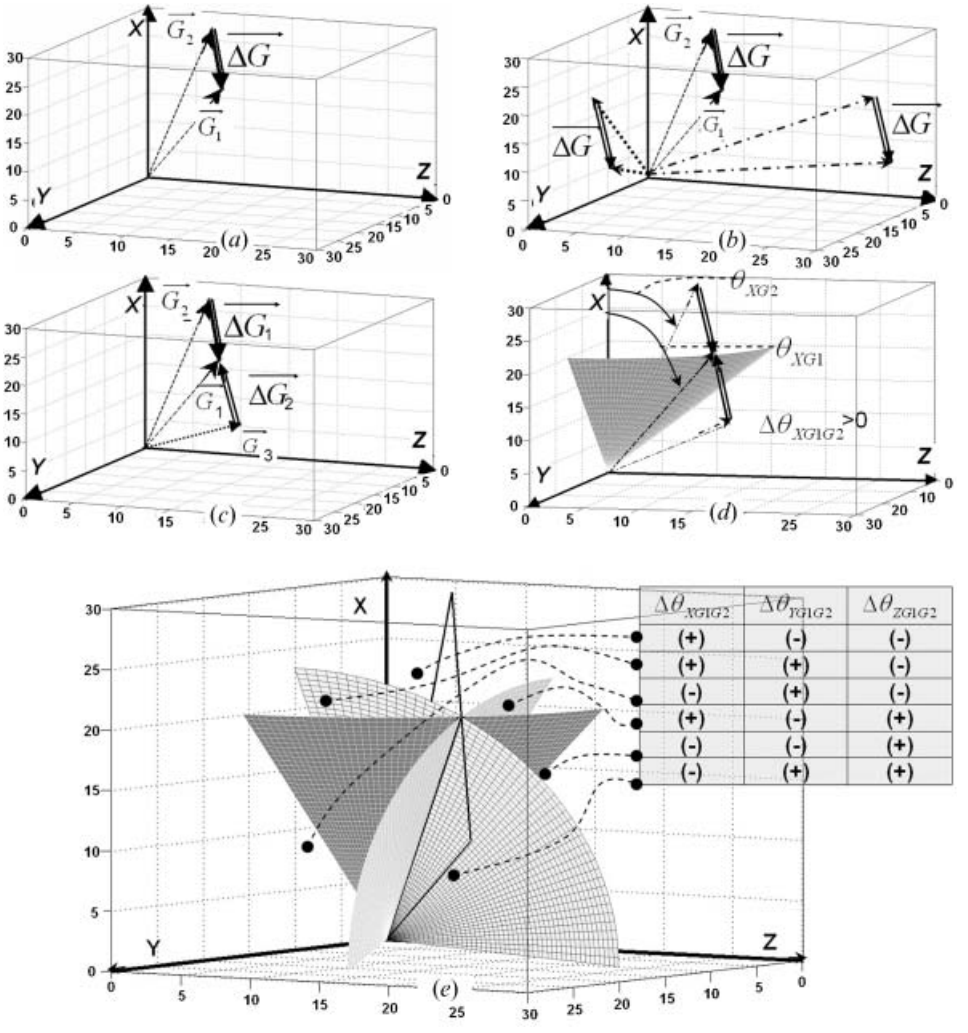

Figure 1. (*a*) The change vector $\overrightarrow{\Delta G}$ as represented in three-dimensional feature space. (*b*) Change vectors $\overrightarrow{\Delta G}$ of equal size and direction, representing different land cover change types in the real world. (*c*) The use of quantities (i) $\left|\overrightarrow{G_1}\right|$ (magnitude of vector $\overrightarrow{G_1}=(g_{11}, g_{12}, g_{13})^T$) and (ii) θ_{XG1}, θ_{YG1}, θ_{ZG1} (the direction angles of vector $\overrightarrow{G_1}=(g_{11}, g_{12}, g_{13})^T$) restricts the number of possible change vector solutions to two equally sized vectors $\overrightarrow{\Delta G_1}$ and $\overrightarrow{\Delta G_2}$, pointing in opposite directions. (*d*) The definition and use of the cone surface or equivalently the use of signed quantity $\Delta\theta_{XG1G2}$ divides the feature space into two distinct regions, further restricting the set of change vector solutions to one out of the two vectors $\overrightarrow{\Delta G_1}$ and $\overrightarrow{\Delta G_2}$ of (*c*). (*e*) The signed combinations of quantities $\Delta\theta_{XG1G2}$, $\Delta\theta_{YG1G2}$ and $\Delta\theta_{ZG1G2}$ further divide the feature space into a greater number of identifiable and unique change clusters.

Consider the cone that is created by rotating vector $\overrightarrow{G_1}$ around axis X, using point O(0,0,0) as the pole of rotation. Suppose also that during the rotation, the direction angle θ_{XG1} of vector $\overrightarrow{G_1}$ with respect to axis X is maintained constant (figure 1(*d*)). The resulted conical surface divides the feature space into two distinct subspaces, each having the following characteristics. For any vector $\overrightarrow{G_2}$ falling in

the interior of the cone, the direction angle θ_{XG2} is definitely smaller than angle θ_{XG1} and therefore the quantity $\theta_{XG1}-\theta_{XG2}$, denoted as $\Delta\theta_{XG1G2}$, is positive (figure 1(*d*)). Similarly, for any vector $\overrightarrow{G_2}$ falling in the exterior of the cone, the corresponding angle difference, denoted as $\Delta\theta_{XG1G2}$, is negative. It can therefore be deduced that the implementation of the conical surface results in a further subdivision of the feature space by creating two new subspaces or clusters. Furthermore, each cluster is assigned a unique characteristic, the sign of quantity $\Delta\theta_{XG1G2}$. This signed quantity can only be positive or negative depending on the pointing direction of change vector $\overrightarrow{\Delta G}$ with respect to the conical surface. Therefore, using the signed quantity $\Delta\theta_{XG1G2}$ as an additional element in the clustering of $\overrightarrow{Z}$ would determine the selection of one out of the two change vector solutions, denoted as $\overrightarrow{\Delta G_1}$ and $\overrightarrow{\Delta G_2}$ in figure 1(*c*). Clearly the characteristic element that is required for the final decision is the algebraic sign of quantity $\Delta\theta_{XG1G2}$.

Considering further the other two conical surfaces formed by rotating vector $\overrightarrow{G_1}$ around axes Y and Z, respectively, the image space is divided into a larger number of subspaces or clusters as shown in figure 1(*e*). Each cluster area is assigned a unique triplet of algebraic signs, as far as the signs of quantities $\Delta\theta_{XG1G2}$, $\Delta\theta_{YG1G2}$ and $\Delta\theta_{ZG1G2}$ are concerned (figure 1(*e*)). These triplets of signs are drawn from the set [(+,+,−), (−,−,+), (+,−,−), (−,+,−), (+,−,+), (−,+,−)]. It follows that the larger the dimension '*n*' of input vector $\overrightarrow{G_1}$, the greater the number of distinct clusters the feature space is divided by the implemented cones. Whatever the number *n*, each cluster is assigned a characteristic and unique combination of signed elements as far as quantities $\Delta\theta_{X_1G1G2}$, $\Delta\theta_{X_2G1G2}$, $\Delta\theta_{X_3G1G2}$, ..., $\Delta\theta_{X_nG1G2}$ are concerned.

According to the proposed method, the change class identification problem is resolved first by clustering the enhanced feature space $\overrightarrow{Z}$ and then labelling the derived clusters. From the previous analysis and considering a three-dimensional image space, the measurement vector $\overrightarrow{Z}$ for a pixel consists of 11 elements, namely the magnitude and the three direction angles of vector $\overrightarrow{G_1}$, the magnitude and the three direction angles of change vector $\overrightarrow{\Delta G}$, and the three signed quantities $\Delta\theta_{XG1G2}$, $\Delta\theta_{YG1G2}$ and $\Delta\theta_{ZG1G2}$. Table 1 describes the 11 elements of measurement vector $\overrightarrow{Z}$ in a three-dimensional image space. As a conclusion, if *n* denotes the dimension of the image space, the size of measurement vector $\overrightarrow{Z}$ for a pixel is $3n+2$.

Table 1. The definition of measurement vector $\overrightarrow{Z}$ in a three-dimensional image space.

$\overrightarrow{Z}=$		
$\left\lvert\overrightarrow{\Delta G}\right\rvert$	$\overrightarrow{\Delta G}$	Magnitude of change vector
$\left\lvert\overrightarrow{G}\right\rvert$	$\left\lvert\overrightarrow{G}\right\rvert$	Magnitude of vector $\overrightarrow{G}$ (in Date 1 or Date 2).
θ_{XG}	θ_{XG}	Direction angle of vector $\overrightarrow{G}$ with respect to the X-axis
θ_{YG}	θ_{YG}	Direction angle of vector $\overrightarrow{G}$ with respect to the Y-axis
θ_{ZG}	θ_{ZG}	Direction angle of vector $\overrightarrow{G}$ with respect to the Z-axis
$\Delta\theta_{XG}$	$\Delta\theta_{XG}$	Difference of direction angles θ_{XG} of vectors $\overrightarrow{G_i}$; i=[1, 2]
$\Delta\theta_{YG}$	$\Delta\theta_{YG}$	Difference of direction angles θ_{YG} of vectors $\overrightarrow{G_i}$; i=[1, 2]
$\Delta\theta_{ZG}$	$\Delta\theta_{ZG}$	Difference of direction angles θ_{ZG} of vectors $\overrightarrow{G_i}$; i=[1, 2]
c_{XG}	c_{XG}	Direction angle of vector $\overrightarrow{\Delta G}$ with respect to the X-axis
c_{YG}	c_{YG}	Direction angle of vector $\overrightarrow{\Delta G}$ with respect to the Y-axis
c_{ZG}	c_{ZG}	Direction angle of vector $\overrightarrow{\Delta G}$ with respect to the Z-axis

It is noteworthy that the calculation of measurement vector $\overrightarrow{Z}$ is fully automatic. The processing of a multitemporal image set comprising two image acquisitions would require only a few hours on a common Pentium computer. The algorithm for the calculation of vector $\overrightarrow{Z}$ for a pixel has been developed using Visual Fortran programming tools.

Should the number of input bands n be too high, the image space could be reduced by either keeping the most relevant and uncorrelated bands or using adequate band transformations (e.g. principal components, vegetation indexes) and then proceed with the calculation of vector $\overrightarrow{Z}$ in the reduced image space. This simplifies the process and reduces considerably the computing requirements for each satellite scene. To efficiently handle the image space in the classification experiments conducted in this research study, only a subset of the available Landsat Thematic Mapper (TM) and Enhanced TM Plus (ETM+) bands was used. This subset was drawn from bands 3, 4 and 5, sensitive to red, infrared and shortwave infrared spectral areas, respectively (see section 4).

3.2 *Thresholding for 'change/no-change' pixel identification*

The accurate and reliable identification of 'change' and 'no-change' pixels depends on several factors, such as the precise radiometric and geometric registration of the two images, the temporal matching in the acquisition of the two images and the proper definition of threshold T as far as the change vector magnitude parameter is concerned. The definition of T is an empirical and subjective procedure. T is usually a single value and applies to the entire difference image $\left|\overrightarrow{\Delta G}\right| = \sqrt{\delta g_1^2 + \delta g_2^2 + \ldots + \delta g_n^2}$ at pixel level. During processing, the change magnitude $\left|\overrightarrow{\Delta G}\right|$ is compared with T and the pixel is assigned the label 'change' or 'no-change' label if $\left|\overrightarrow{\Delta G}\right|$ is greater or less than T. As can be inferred, the greater the difference between $\left|\overrightarrow{\Delta G}\right|$ and T, the higher the user confidence in separating the 'change' from the 'no-change' areas. If, on the contrary, $\left|\overrightarrow{\Delta G}\right|$ and T are similar to each other, the outcome is ambiguous and the final decision is subject to further refinement by the user.

However, it is possible that the 'change/no-change' pixel classification is erroneous, even when the difference between $\left|\overrightarrow{\Delta G}\right|$ and T is large. This can occur on transition from a 'change' to a 'no-change' area. In practice, the spectral properties of the pixels located close to the limit and inside a 'no-change' area are very influenced by the neighbouring 'change' pixels. This can lead to pixels being erroneously identified as 'change' pixels. This problem is broadly known as change area overestimation and becomes particularly prominent when the two images are compared at a single-pixel level.

Change area overestimation can also be the result of image misregistration. Even though subpixel registration of the two images is a prerequisite for a change detection study, it might be the case that a greater geometric shift exists in certain areas. This cannot be easily observed as it arises locally and its size does not exceed 1 pixel or, at the maximum, 1.5 pixels. In some cases this problem cannot be resolved because of limitations in the quality and adequacy of the data used for image rectification and image registration (e.g. precision of the digital elevation model (DEM), control point abundance and accuracy).

To efficiently address the problem of change area overestimation, we considered it necessary to take evidence derived from the pixel's geographic neighbourhood into account. In the framework of this research study, the pixel's geographic context was defined as a 3×3 pixel kernel. This was achieved by calculating the spectral vector differences $\left|\overrightarrow{\Delta G_{ij}}\right|$ between any pixel i on the first image and the corresponding nine (3×3) pixels j (j=1 to 9) located in the immediate neighbourhood of pixel i on the second image. Comparison of the nine $\left|\overrightarrow{\Delta G_{ij}}\right|$ values with T gives nine distinct pieces of evidence for pixel i of the 'change' or 'no-change' type. According to the proposed approach, pixel i is identified as 'change' when all nine bits of evidence, associated with the pixel fully support this decision. In the opposite case the pixel is identified as 'no-change'. Furthermore, a measure indicating the degree of confidence of this decision is calculated and adequately stored in a separate information layer. This measure is directly linked to the number of occurrences a pixel has been identified as 'no-change'. Thus, its value varies between 1/9 and 1. The final decision is left to the analyst, who has to decide which level of confidence to rely on when 'change' and 'no-change' areas are to be mapped.

The proposed algorithmic approach can be summarized as follows. Consider two images denoted as 'reference' and 'slave' images, respectively. Let the size of the images be $L \times E$, where L denotes the number of lines and E the number of pixels per line. The reference image is scanned pixel by pixel and then line by line. For any reference pixel i located at coordinates (l, e), the algorithm considers a 3×3 window centred at the same location on the slave image (see figure 2). Then:

i. Calculate magnitude $\left|\overrightarrow{G_i}\right|$ of 'reference' pixel i.
ii. Calculate magnitudes $\left|\overrightarrow{G_j}\right|$ of the nine 'slave' pixels j (j=1 to 9) inside the 3×3 kernel.
iii. Calculate the magnitudes of the nine change vectors $\overrightarrow{\Delta G_{ij}}$.
iv. Arbitrarily set reference pixel i to 'change'.
v. Compare the magnitudes of change $\left|\overrightarrow{\Delta G_{ij}}\right|$ with T.
vi. If the current value of $\left|\overrightarrow{\Delta G_{ij}}\right|$ is $\leqslant T$, then:

a. change the label of reference pixel i to 'no-change'.
b. increase the degree of user confidence in this decision by 1.

vii. Repeat step (vi) until the complete set of magnitudes $\left|\overrightarrow{\Delta G_{ij}}\right|$ is processed.
viii. Increase the reference pixel counter by 1.
ix. Repeat steps (i) to (viii) until the reference pixel counter equals 'E'.
x. Increase the line counter by 1.
xi. Stop processing when line counter equals 'L' and pixel counter equals 'E'.
xii. Remove from the resulting 'change/no-change' map any remaining object that is smaller than a user-defined Minimum Mapping Unit (MMU).

Figure 3 shows the result of the application of the proposed thresholding approach on two Landsat TM and ETM+ images acquired over Athens (Greece) in 1990 and 2000, respectively (source: the Hellenic Cadastral and Mapping Organization of Greece, HEMCO). The two images have been used as input in the framework of the CLC2000 and CLC-Change projects in Greece. Comparing the map in figure 3 with the one in figure 6(*b*), it becomes obvious that the resulting 'change/no-change' map is similar to the one generated in the framework of the CLC2000-Greece project by visual

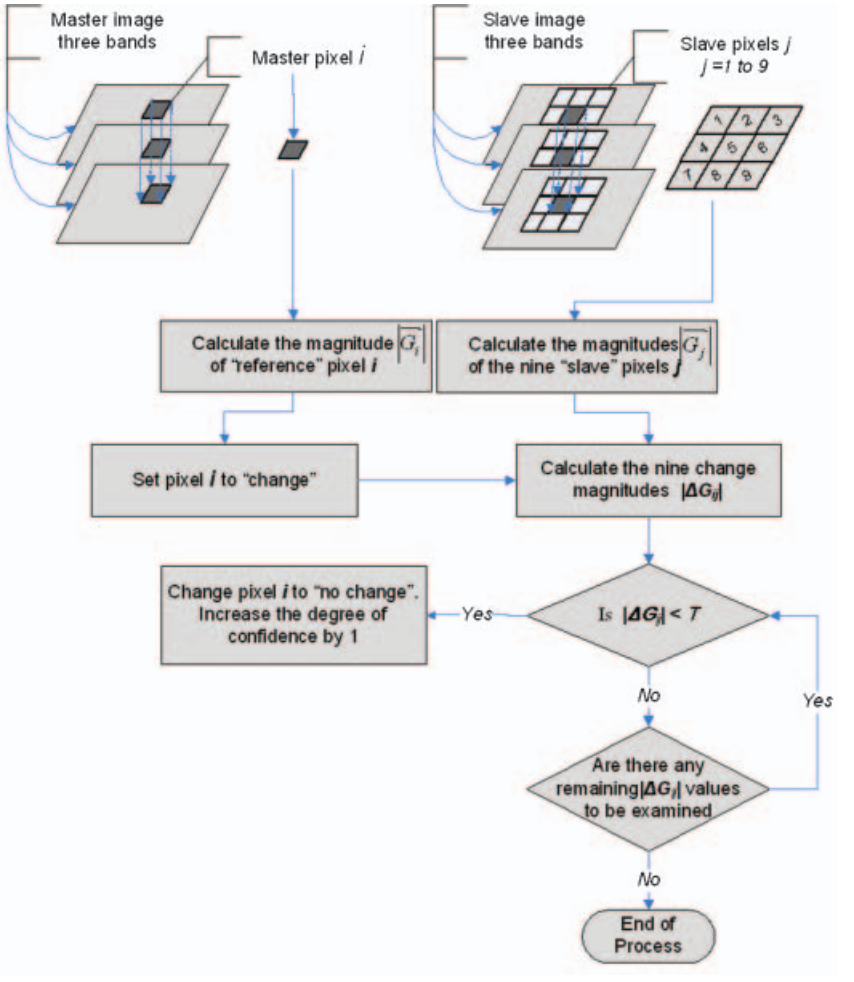

Figure 2. Flowchart of the kernel-based thresholding method to map change/no-change pixels.

image interpretation. Moreover, as shown in table 6, the map resulting from the proposed thresholding approach is accurate by 88.3% compared to the visual image interpretation map illustrated in figure 6(*b*) (see also section 4.3).

3.3 *Clustering the* $(3n+2)$*-dimensional feature space*

Clusters of change types were defined by creating groups of similar vectors $\vec{Z}$ in the $(3n+2)$-dimensional feature space. For this purpose the ISODATA unsupervised clustering algorithm of ERDAS Imagine was used. Clustering results were checked visually and each cluster was assigned a unique change label of the 'from-to' type. Using the labelled clusters as signatures, the maximum likelihood classification algorithm of ERDAS Imagine was invoked and all 'change' pixels were classified into a single change class. The ERDAS Imagine classification algorithm practically produced as many classification layers as the number of signatures used. Each classification layer was assigned a distance measure layer, representing the pixels' best classification in descending order; in other words, layer 1 contained the pixels' labels for the best classification, layer 2 those for the second best, and so on.

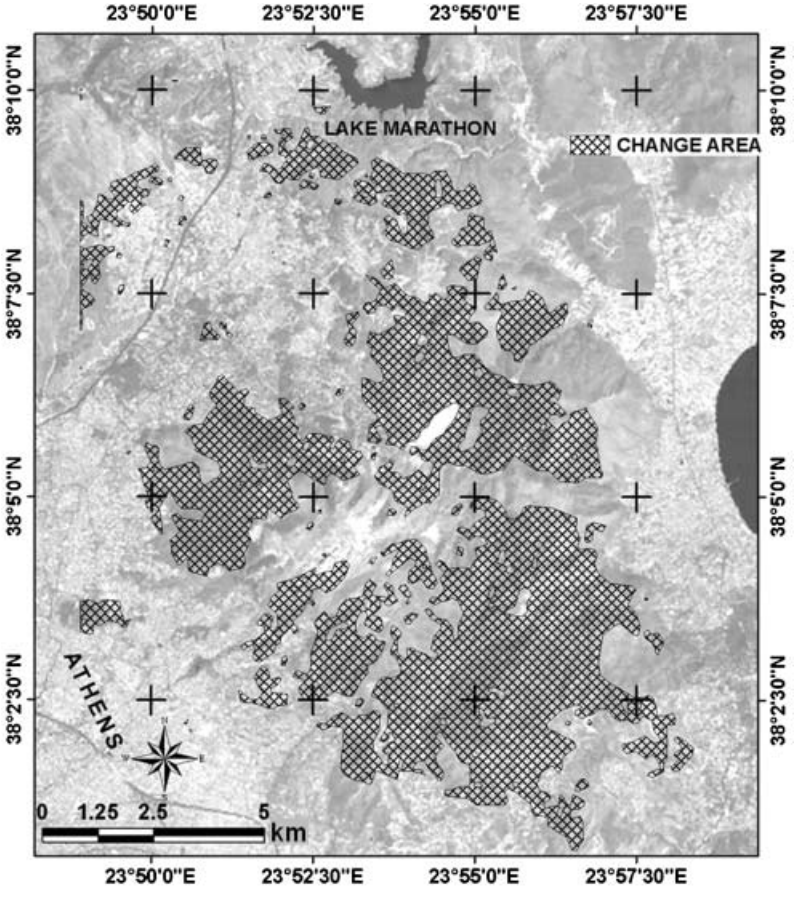

Figure 3. Change/no change pixel map resulting from the kernel-based thresholding method. This change/no-change map is similar to the one derived by visual image interpretation in the framework of the CLC-Change project in Greece (figure 6(*b*)).

4. Implementation of the proposed method

4.1 *The Ptolemais test area*

The 870 km^2 study area is located northeast of the city of Ptolemais in Kozani, east of the city of Amindeo in Florina, southeast of the lake Vegoritida and west of the city of Naousa in Imathia (figure 4(*a*)). It lies in the valley of Eordaia and on the slopes of Mount Vermio to the northeast. The south part of the area near Ptolemais is known for its coalmines and power supply stations. Four power stations producing 70% of the country's electricity and the coalmines to power them are located in the area. Considerable landscape changes are visible around the lignite mining areas due to continuous extraction of coal and recultivation of the exploited areas. Mount Vermio, with a north–south orientation and elevations ranging from 500 to 2100 m, is located on the eastern side of the test area. The mountain slopes are characterized by highly productive forest ecosystems that are favoured by the pluvial aerial masses coming from the Aegean Sea. Several plant species such as *Pinus nigra*, *Abies borissi-regis*, *Castanea sativa*, *Ilex aquifolium*, *Juniperus*, *Quercus*, *Salix*, *Populus*, *Platanus*, *Acer*, *Fraxinus*, *Buxus sempervirens*, *Cornus*, *Prunus* and *Robus* are found in these mountain

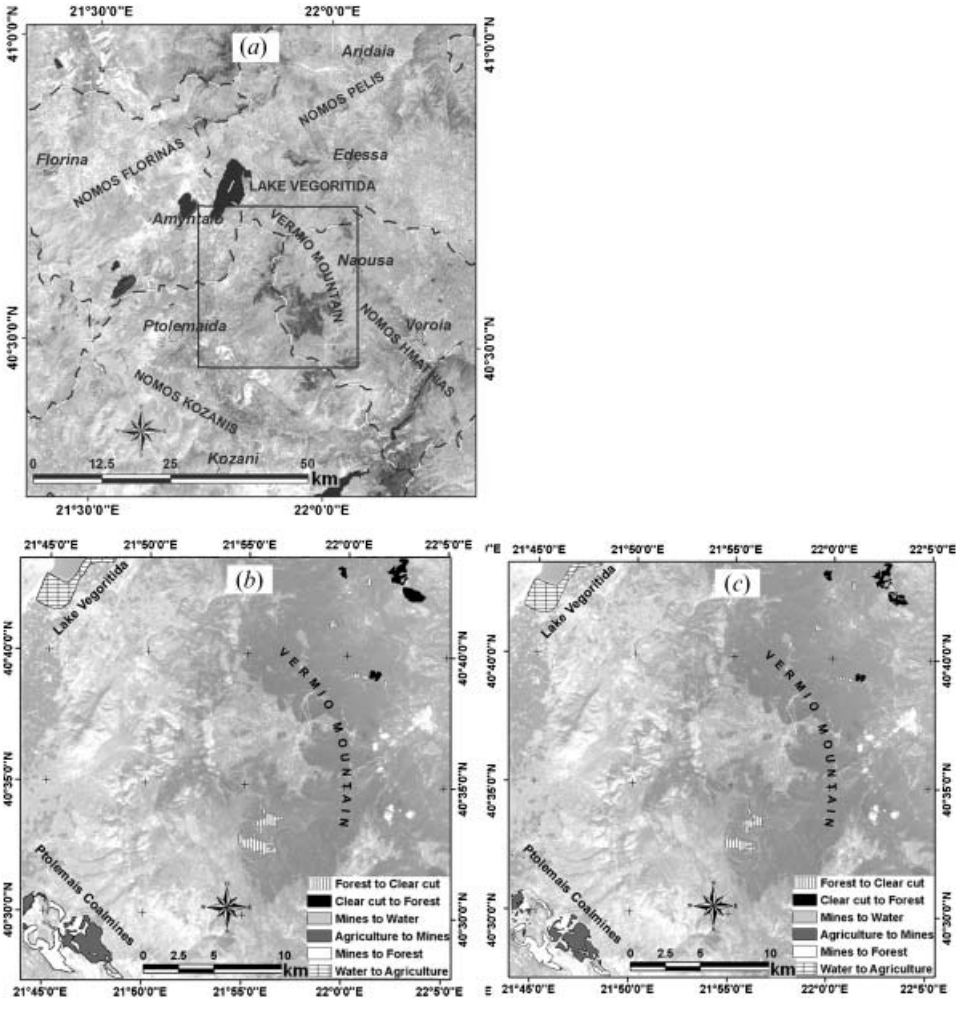

Figure 4. (*a*) The Ptolemais test area. (*b*) Land cover change map of the study area delivered in the framework of the ESA/GSE FM project. (*c*) Land cover change map generated by the proposed CVA method.

ecosystems. Due to the disturbed history of the forested zones, which is historically related to clearcuts, heavy exploitation and fire occurrences, a significant number of land cover changes are reported in the test area.

Lake Vegoritida is located in the north of the study area. It represents a very sensitive and disturbed ecosystem due to wetland degradation and water pollution. The water level gets lower every year because of water overpumping by the power supply stations, intense agricultural irrigation, physical leakage and drought. The transformation of wetland areas to agricultural land is today a very common type of change in the area around the lake.

The Ptolemais test site was initially studied in the framework of the ESA/GMES Service Element Forest Monitoring (ESA/GSE FM) project. The aim of the ESA/GSE FM project is to implement a set of standardized remote sensing services for

qualified forest classifications and forest change assessments all over Europe. The outcome of the GSE/FM project was an accurate land cover change map of the area of interest, validated and refined through visual image interpretation using existing 1 : 5000-scale orthophoto maps and *in situ* collected data. This reference product shown in figure 4(*b*) was used as a basis to estimate the accuracy level of the proposed change classification method. The corresponding accuracy figures are summarized in tables 2 and 3. The land cover change classification generated by the proposed CVA method is illustrated in figure 4(*c*). It is noteworthy that the two Landsat TM scenes (path/row: 184/032, 7 July 1990 and 5 August 2002) that were used in the framework of the ESA/GSE FM project were also used for the purposes of this analysis. The study concludes that the changes identified and mapped during the 1990–2002 period are characterized by three main aspects:

(1) Changes in tree vegetation status on the slopes of Mount Vermio. These relate to deforestation and reforestation activity, extensive forest exploitation and subsequent post-exploitation forest regeneration. Therefore, two types of change are reported, ranging from class forest to clearcuts, as well as from clearcuts to regenerated forested areas. The two changes are of similar size (approximately 1717 ha for the former and 1280 ha for the latter).
(2) Agricultural land expansion in the north part of the study area by encroaching upon fields that used to be flooded by Lake Vegoritida. The agricultural land has been extended for approximately 2570 ha on the dried parts of the lake surface.
(3) Land cover changes in the coalmine areas located in the north of the city of Ptolemais. In the context of these areas there are three types of change reported: (*a*) from agricultural land to newly opened mine fields or bare soils (2700 ha); (*b*) from bare soils and old mines to reforested areas after rehabilitation of the exploited mine parts (2010 ha), and (*c*) from bare soils and old mine areas to artificial lakes (345 ha).

The performance of the proposed CVA method was assessed by estimating the change detection accuracy at both 'change/no-change' and 'from-to' change detection levels. Tables 2 and 3 show the corresponding error matrices derived by comparing the outcome of the proposed CVA method with the reference map generated in the framework of the ESA/GSE FM project. These tables show that the overall accuracy achieved for the 'change/no-change' and 'from-to' change class detection was of the order of 96.1% and 95.9%, respectively. These figures, along with the corresponding

Table 2. Accuracy assessment of 'change/no-change' detection using the proposed CVA method: the Ptolemais case study.

	Classified change: CVA (in pixels)			
Reference change: photointerpretation (in pixels)	Change pixels	No-change pixels	Sum	Producer's accuracy (%)
Change pixels	95 238	22 878	118 116	80.6
No-change pixels	14 693	833 444	848 137	98.3
Sum	109 931	856 322	966 253	
User's accuracy (%)	86.6	97.3		
Overall accuracy=96.1%				

Table 3. Accuracy assessment of 'from-to' change detection using the proposed CVA method: the Ptolemais case study.

Reference 'from-to' change classes: image interpretation results (in pixels)	Classified 'from-to' change classes (in pixels)								
	No-change	1	2	3	4	5	6	Sum	Producer's accuracy (%)
No-change	833 444	4379	1575	1585	5365	1283	506	848 137	98.3
1	4647	14 130	96	0	189	0	25	19 087	74.0
2	2874	0	11 179	0	33	109	0	14 195	78.8
3	591	0	0	3245	0	0	0	3836	84.6
4	7554	1101	0	0	21 376	87	5	30 123	71.0
5	5596	0	0	14	0	16 722	5	22 337	74.9
6	1616	0	0	0	0	0	26 922	28 538	94.3
Sum	856 322	19 610	12 850	4844	26 963	18 201	27 463	966 253	
User's accuracy (%)	97.3	72.1	87.0	67.0	79.3	91.9	98.0		
Overall accuracy=95.9%									

Change classes: (1) forest to clearcuts; (2) clearcuts to forest; (3) mine areas or bare soil to inland water; (4) agricultural land to mine open fields or bare soil; (5) mine areas to forestland (area rehabilitation); (6) inland water to agricultural land.

user's and producer's accuracy levels, which range from 72% to 98%, indicate that the proposed method is effective for change-type discrimination.

4.2 *The Thassos test area*

The test area is the island of Thassos in the prefecture of Kavala. Thassos is the most northerly island in the Aegean Sea (see figure 5(*a*)). It extends from 24°30′ to 24°48′ E and 40°33′ to 40°49′ N and has a total surface area of 384 km^2. The island

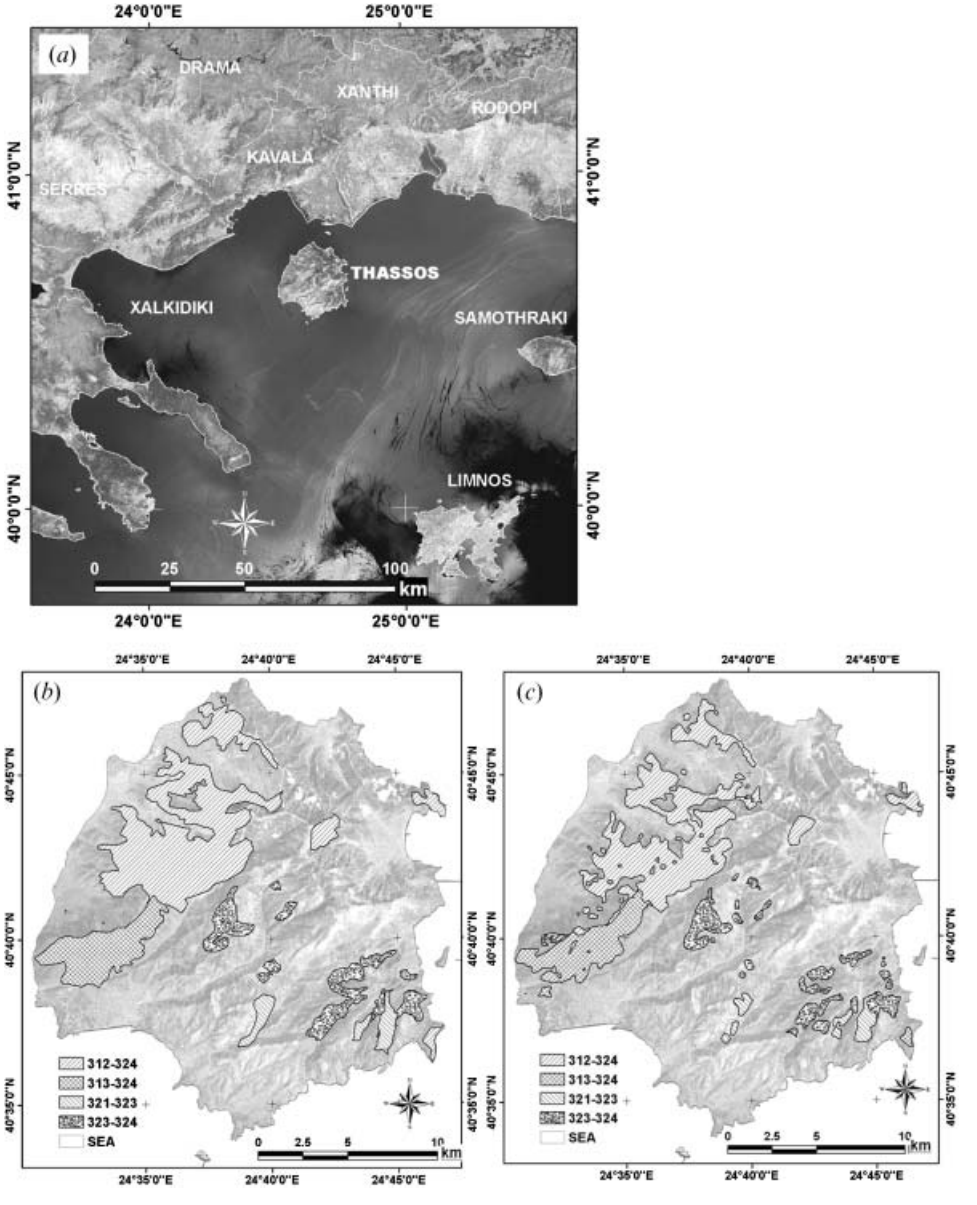

Figure 5. (*a*) The Thassos test area. (*b*) Land cover change map of the island of Thassos delivered in the framework of the CLC-Change project. (*c*) Land cover change map of the island of Thassos generated by the proposed CVA method.

is mountainous with intense relief and a variety of landscapes. Elevation ranges from sea level to 1217 m and the terrain slopes range from 0° to 76°. It belongs to the Mediterranean vegetation eco-zone characterized by thermophile broad-leaved evergreen shrubs, pure stand forests of *Pinus brutia* and *Pinus nigra* and a significant number of rare species and wild plants. In the past there were stands of *Abies borisii regis* but these have been destroyed by wildfires over the past years. The hardwoods are limited to small rivers, swamps and streams and they consist of *Platanus orientalis* as well as wild chestnut stands. Apart from forested vegetation, other types of schlerophylous Mediterranean vegetation are found, such as maquis and garrigue. In the interior valleys most of the surface is grazed. Considerable agricultural activity is focused on cereal, vegetable, fruit, vineyard and olive production.

Due to its natural beauty the island has been one of the preferred tourist destinations in Greece. Apart from tourism, which mainly affects coastal areas, agriculture and mining also result in land cover changes. Within the forested land, significant changes mainly involve extensive exploitation of the natural ecosystems. Furthermore, the three large catastrophic fire events that occurred in the 1984–2000 period have led to the loss of thousands of hectares of *Pinus brutia* and *Pinus nigra* forests (Mitri and Gitas 2006). For all these reasons the island of Thassos has been identified as an ideal case for addressing the objectives of this study and evaluating the performance of the proposed method.

The CLC-Change database introduces a change surface of about 85.5 km^2, representing approximately 22.3% of the island's territory. The two Landsat TM/ETM+ images (scene path/row 183/032) acquired over the island of Thassos on 10 August 1992 and 11 August 2001 that were used in the framework of the CLC-Change project were also used in this analysis. The following change classes of the 'from-to' type are reported in the corresponding CLC-Change database:

(1) Class 312–324: from coniferous forest to transitional woodland shrub. The change area surface equals 5181 ha.
(2) Class 313–324: from mixed forests to transitional woodland shrub. The change area surface equals 1484 ha.
(3) Class 323–324: from sclerophyllous vegetation to woodland shrub. The change area surface equals 1407 ha.
(4) Class 321–323: from natural grassland to sclerophyllous vegetation. The change area surface equals 498 ha.

The result of the proposed CVA method is illustrated in figure 5(*c*), while the visual image interpretation output generated in the framework of the CLC-Change project is shown in figure 5(*b*). The similarity of the two results becomes obvious. Tables 4 and 5 summarize the accuracy figures for 'change/no-change' and 'from-to' change class detection. As reported, the overall accuracy achieved for the 'change/no-change' and 'from-to' change class detection was of the order of 91.4% and 91%, respectively. The figures for user's and producer's accuracy along with the figures of overall accuracy confirm a clear potential in the use of the proposed automatic approach in operational projects. The CVA results conform to the precision requirements of the CLC2000-Greece project and ensure the cost efficiency of operations.

4.3 *The Athens test area*

This 270 km^2 test area is located northeast of the city of Athens (figure 6(*a*)). It comprises a complex and fragmented landscape environment, highly disturbed by

Table 4. Accuracy assessment of 'change/no-change' detection using the proposed CVA method: the Thassos case study.

	Classified change: CVA (in pixels)			
Reference change: photointerpretation (in pixels)	Change pixels	No-change pixels	Sum	Producer's accuracy (%)
Change pixels	99 210	37 942	137 152	72.3
No-change pixels	14 956	463 458	478 414	96.9
Sum	114 166	501 400	615 566	
User's accuracy (%)	86.9	92.4		
Overall accuracy=91.4%				

intensive construction activity and infrastructure works. In recent years the urban land has expanded rapidly in the urban–rural fringe area by encroaching upon areas that used to be covered by arable crops, vineyards, broad-leaved and coniferous forests, grasslands, sclerophyllous vegetation and shrubs. Mount Penteli, which is located at the northeast of the test area, was repeatedly hit by wildfires in 1995 and 1998, during which more than 10 000 ha of *Pinus halepensis* forest cover was burnt. Due to these frequent fire events the landscape patterns and the floristic composition of the existing plant communities were greatly affected and the plant community structure and diversity on mountain slopes were changed. Fieldwork has revealed that 33% of the previously existing species have disappeared under the frequent fire regime, while 16% new taxa of the type *Herbaceous compositae* have appeared (Arianoutsou 2001).

The study of the CLC-Change database shows a 15% reduction of forested areas, which have changed to transitional woodlands and shrublands. Moreover, a construction site growth of approximately 2% at the expense of pre-existing agricultural, transitional woodland, shrubland and forested areas has been documented. According to the CLC-Change database, six distinct types of change classes within the former forested and semi-forested zones of the test area are reported, as follows:

(1) Class 311–324: from broad leaved forests to transitional woodland shrub. The change area surface equals 223 ha.
(2) Class 312–324: from coniferous forest to transitional woodland shrub. The change area surface equals 3803 ha.
(3) Class 243–133: from agricultural land to construction sites. The change area surface equals 26 ha.
(4) Class 312–133: from coniferous forest to construction sites. The change area surface equals 143 ha.
(5) Class 324–133: from transitional woodland shrub to construction sites. The change area surface equals 125 ha.
(6) Class 324–312: from transitional woodland shrub to coniferous forest. The change area surface equals 218 ha.

The implementation and assessment of the proposed CVA method in the test area of Athens was based on two Landsat TM/ETM+ scenes acquired in March 1990 and July 2000, respectively (scene path/row: 183/033). The image of 1990 was found in the archive of HEMCO. The outcome of the CLC-Change project, result of visual image interpretation of the two Landsat TM/ETM+ image acquisitions, is

Table 5. Accuracy assessment of 'from-to' change detection using the proposed CVA method: the Thassos case study.

Reference 'from-to' change classes: image interpretation results (in pixels)	Classified 'from-to' change classes: CVA results (in pixels)						
	No-change	312 to 324	313–324	321 to 323	323 to 324	Sum	Producer's accuracy (%)
No-change	463 458	7478	2211	629	4638	478 414	96.9
312 to 324	24 558	57 216	1129	0	2	82 905	69.0
313 to 324	2916	905	19 923	1	0	23 745	83.9
321 to 323	2567	1	0	5228	185	7981	65.5
323 to 324	7901	11	2	160	14 447	22 521	64.1
Sum	501 400	65 611	23 265	6018	19 272	615 566	
User's accuracy (%)	92.4	87.2	85.6	86.9	75.0		
Overall accuracy=91.0%							

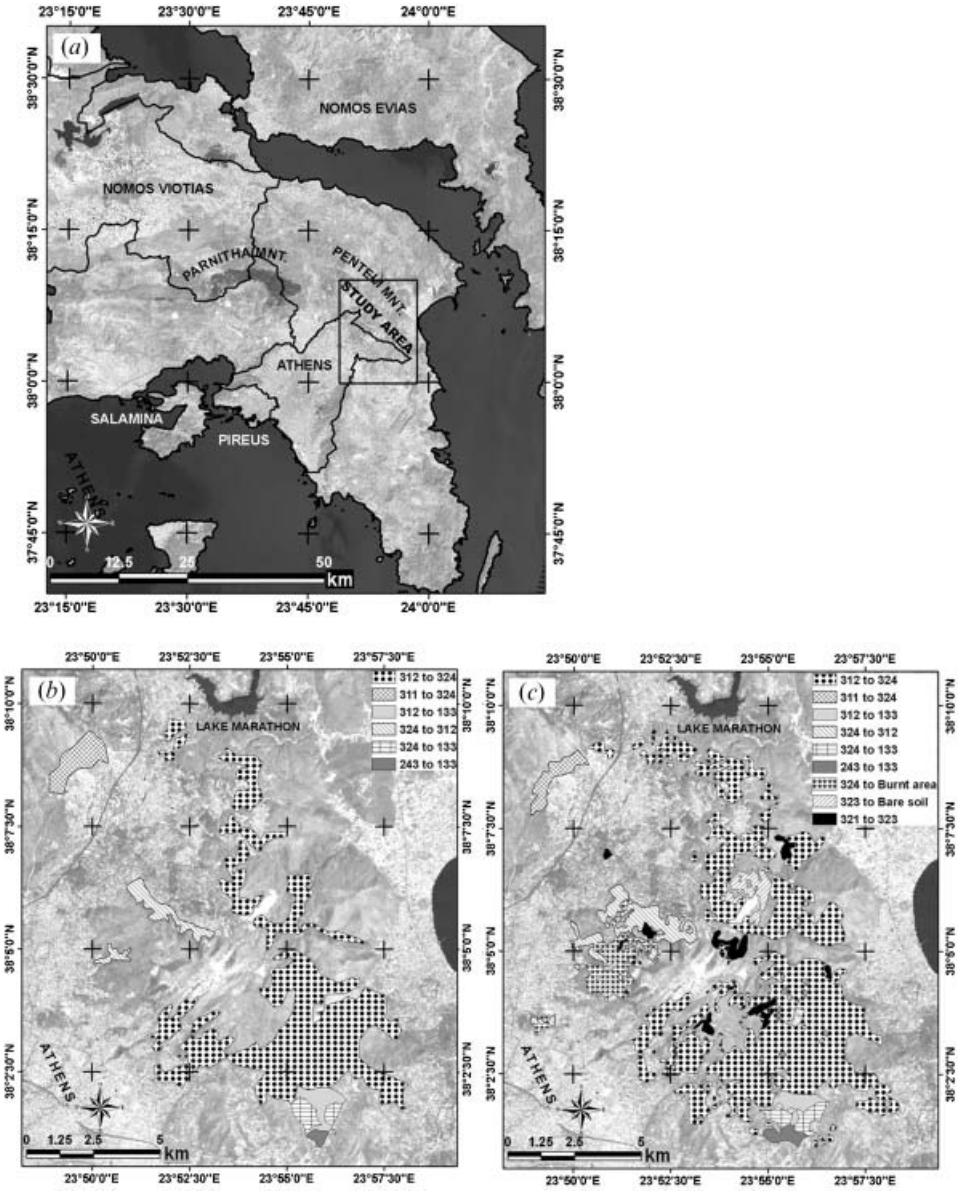

Figure 6. (*a*) The Athens test area. (*b*) Land cover change map of the study area delivered in the framework of the CLC-Change project. (*c*) Land cover change map generated by the proposed CVA method.

illustrated in figure 6(*b*). Figure 6(*c*) illustrates the analysis results according to the proposed CVA methodology. The two figures are similar as the changes depicted present almost the same characteristics (surface, type and location). The CVA results conform to the visual image interpretation assessments. According to the proposed CVA method, the change areas correspond to 18.4% of the total test area, whereas, according to the visual image interpretation results, the change areas correspond to 14.2% of the study area.

To evaluate the performance of the proposed method, accuracy assessments of the detected changes were estimated both at the 'change/no-change' and 'from-to' change class detection levels. Tables 6 and 7 show the corresponding error matrices. These matrices were produced by cross-correlating at the pixel level the CVA map with the map produced by visual image interpretation. As shown in tables 6 and 7, the overall accuracy achieved using the proposed CVA method for 'change/no-change' and 'from-to' change class detection was of the order of 88.3% and 87.9%, respectively. The levels of user's and producer's accuracy as well as the overall accuracy figures shown in tables 6 and 7 demonstrate the potential of the proposed method.

5. Discussion and conclusions

The establishment of a realistic European policy in the environment sector requires consistent and comparable land cover data across the continent. As part of this mandate, the EC has been implementing the CLC and the CLC-Change projects with the aim of regularly updating the relevant databases throughout Europe. In Greece, the CLC-Greece project has been implemented twice. Project operations have been based on the interpretation of multidate Landsat TM and ETM + images covering the entire country. The identification and labelling of land cover classes and land cover change classes through visual interpretation has turned out to be a laborious task. Significant effort has been required to locate changes that were close to the MMU specified for the project (5 ha).

In an attempt to limit excessive time and effort requirements, an automatic approach was implemented and tested in the framework of this research. The proposed approach makes use of a measurement vector $\vec{Z}$ that incorporates information on land cover types and land cover change characteristics according to the CVA method. Measurement vector $\vec{Z}$ becomes subject to unsupervised clustering and the derived change clusters are fed as signatures to a supervised classification algorithm to generate the final 'from-to' type change classifications. The method was proven to adequately serve the objectives of operational projects. It is completely automatic and considerably limits the data processing effort, while the quality of the returned change classifications remains high. The use of a kernel approach in 'change/no-change' area delineation eliminates meaningless changes of just a few pixels from the final classification.

Table 6. Accuracy assessment of 'change/no-change' detection using the proposed CVA method. The Athens case study.

	Classified change: CVA (in pixels)			
Reference change: photointerpretation (in pixels)	Change pixels	No-change pixels	Sum	Producer's accuracy (%)
Change pixels	44 974.0	15 921.0	60 895.0	73.9
No-change pixels	34 085.0	333 855.0	367 940.0	90.7
Sum	79 059.0	349 776.0	428 835.0	
User's accuracy (%)	56.9	95.4		
Overall accuracy=88.3%				

Table 7. Accuracy assessment of 'from-to' change detection using the proposed CVA method: the Athens case study.

Reference 'from-to' change classes: image interpretation results (in pixels)	Classified 'from-to' change classes: the CVA method results (in pixels)											
	No-change	312 to 324	311 to 324	312 to 133	324 to 312	324 to 133	243 to 133	324 to burnt	323 to bare soil	321 to 323	Sum	Producer's accuracy (%)
No-change	333 855	20 603	542	20	3831	517	21	4282	1909	2360	367 940	90.7
312 to 324	12 666	35 693	0	62	26	0	0	496	137	199	49 279	72.4
311 to 324	2046	9	1612	0	0	0	0	0	0	0	3667	44.0
312 to 133	165	299	0	1455	0	193	33	0	0	0	2145	67.8
324 to 312	791	9	0	0	2379	0	0	172	0	5	3356	70.9
324 to 133	153	8	0	119	0	1610	58	0	0	0	1948	82.6
243 to 133	100	32	0	0	0	1	367	0	0	0	500	73.4
324 to burnt	0	0	0	0	0	0	0	0	0	0	0	0.0
323 to bare soil	0	0	0	0	0	0	0	0	0	0	0	0.0
321 to 323	0	0	0	0	0	0	0	0	0	0	0	0.0
Sum	349 776	56 653	2154	1656	6236	2321	479	4950	2046	2564	428 835	
User's accuracy (%)	95.4	63.0	74.8	87.9	38.1	69.4	76.6	0.0	0.0	0.0		

Overall accuracy=87.9%

The automations developed for change detection and labelling become an important asset, as the MMU size for the changed areas tends to be smaller than a threshold depending on the spatial resolution of the satellite data. An example could be the ESA/GSE FM project for which the MMU size for the changed areas was set to 0.5 ha. In such a project there is a high risk for the interpreters to accidentally disregard or omit changes that are close in size to the MMU as being too small. The situation becomes more difficult to the extent that such small-sized changes are numerous and highly dispersed in the study area. In these conditions the use of the suggested automatic method can be a valuable help as it provides the ability to detect and label all identifiable changes occurring in the study area, regardless of their size and shape.

Another advantage of the suggested method is the possibility for simultaneous use of a multitude of input layers. At this point the reader should note that the size of feature space $\vec{Z}$ increases by a factor of 3 with the number of input layers. To speed up clustering convergence and achieve an improved clustering performance, it is thus important to compress the feature space dimension by using the most relevant input bands or band transformations (e.g. principal component images, vegetation indexes), depending on the nature of the changes under study. As an example, the detection of changes due to a fire occurrence would preferably make use of bands in the infrared part of the spectrum in proper combination with vegetation index layers. Less significant bands or bands correlated with those already used should be excluded.

In conclusion, the change detection method described in this paper seems to be an effective solution and is recommended for operational projects. It can be run on any common PC and results in robust classifications. Its implementation in the highly fragmented and dynamically changing landscape environments in Greece has resulted in qualified and accurate land cover change maps, achieving an overall level of classification accuracy of 88–96%. Compared to visual image interpretation, the method requires half as much effort. This is justified by examining the relevant metadata reported in the framework of the CLC2000-Greece project. According to these records an average of 8 days' work had been required for processing a 1 : 100 000-scale map representing a 60 km × 40 km area. On the contrary, the proposed automatic CVA method required no more than 4 days, one for data preprocessing and feature space calculation (vector $\vec{Z}$), a second day for data clustering and change class labelling, and one to two additional days for change classification refinement depending upon the nomenclature scheme used.

Acknowledgements

The Hellenic Mapping Cadastral Organization (HEMCO) is thanked for providing support in delivering samples of Landsat TM and ETM+ images together with the corresponding CLC2000-Greece and CLC-Change databases that were required for this research.

References

ARIANOUTSOU, M., 2001, Landscape changes in Mediterranean ecosystems of Greece: implications for fire and biodiversity issues. *Journal of Mediterranean Ecology*, **2**, pp. 165–178.

AVISSAR, R. and PIELKE, R.A., 1989, A parameterization of heterogeneous land surfaces for atmospheric numerical models and its impact on regional meteorology. *Monthly Weather Review*, **117**, pp. 2113–2136.

CHEN, J., GONG, P., HE, C., PU, R. and SHI, P., 2003, Land-use/land-cover change detection using improved change-vector analysis. *Photogrammetric Engineering and Remote Sensing*, **69**, pp. 369–379.

COPPIN, P.R. and BAUER, M.E., 1996, Digital change detection in forest ecosystems with remote sensing imagery. *Remote Sensing Reviews*, **13**, pp. 207–234.

DING, Y., ELVIDGE, C.D. and LUNETTA, R.S., 1998, Survey of multispectral methods for land cover change detection analysis. In *Remote Sensing Change Detection: Environmental Monitoring Change and Applications*, R.L. Lunetta and C.D. Elvidge (Eds), pp. 21–39 (New York, NY: Sleeping Bear Press, Inc.).

EASTMAN, J. and FULK, M., 1993, Long sequence time series evaluation using standardized principal components. *Photogrammetric Engineering and Remote Sensing*, **59**, pp. 1307–1312.

ENGVALL, J.L., TUBBS, J.D. and HOLMES, Q.A., 1977, Pattern recognition of LANDSAT data based upon temporal trend analysis. *Remote Sensing of Environment*, **6**, pp. 303–314.

FUNG, T. and LEDREW, E., 1987, Application of principal component analysis to change detection. *Photogrammetric Engineering and Remote Sensing*, **53**, pp. 1649–1658.

FUNG, T. and LEDREW, E., 1988, The determination of optimal threshold levels for change detection using various accuracy indices. *Photogrammetric Engineering and Remote Sensing*, **54**, pp. 1449–1454.

HAYES, D.J. and SADER, S.A., 2001, Comparison of change-detection techniques for monitoring tropical forest clearing and vegetation regrowth in a time series. *Photogrammetric Engineering and Remote Sensing*, **67**, pp. 1067–1075.

HENDERSON-SELLERS, A. and PITMAN, A.J., 1992, Land surface schemes for future climate models: specification, aggregation, and heterogeneity. *Journal of Geophysical Research*, **97**, pp. 2687–2696.

HOWARTH, P.J. and WICKWARE, G.M., 1981, Procedures for change detection using Landsat digital data. *International Journal of Remote Sensing*, **2**, pp. 277–291.

JENSEN, J.R., RUTCHEY, K., KOCH, M.S. and NARUMALANI, S., 1995, Inland wetland change detection in the everglades water conservation area 2A using a time series of normalized remotely sensed data. *Photogrammetric Engineering and Remote Sensing*, **61**, pp. 199–209.

JOHNSON, R.D. and KASISCHKE, E.S., 1998, Change vector analysis: a technique for the multispectral monitoring for land cover and condition. *International Journal of Remote Sensing*, **19**, pp. 411–426.

LAMBIN, E.F. and STRAHLER, A.H., 1994, Indicators of land cover change for change vector analysis in multi-temporal space at coarser spatial scales. *International Journal of Remote Sensing*, **15**, pp. 2099–2119.

LYON, G.J., DING, Y., LUNETTA, R.S. and ELVIDGE, C.D., 1998, A change detection experiment using vegetation indices. *Photogrammetric Engineering and Remote Sensing*, **64**, pp. 143–150.

MACLEOD, R.D. and CONGALTON, R.G., 1998, A quantitative comparison of change detection algorithms for monitoring eelgrass from remotely sensed data. *Photogrammetric Engineering and Remote Sensing*, **64**, pp. 207–216.

MALILA, W.A., 1980, Change vector analysis: an approach for detecting forest changes with Landsat. In *Proceedings of the 6th Annual Symposium on Machine Processing of Remotely Sensed Data*, 3–6 June, Purdue University, West Lafayette, Indiana (Ann Arbor: ERIM), pp. 326–335.

MARSH, S., WALSH, J., LEE, C., BECK, L. and HUTCHINSON, C., 1992, Comparison of multi-temporal NOAA-AVHRR and SPOT XS satellite data for mapping land cover dynamics in the West African Sahel. *International Journal of Remote Sensing*, **13**, pp. 2997–3016.

MITRI, G.H. and GITAS, I.Z., 2006, Fire type mapping using object-based classification of Ikonos imagery. *International Journal of Wildland Fire*, **15**, pp. 457–462.

NELSON, R.F., 1983, Detecting forest canopy change due to insect activity, using LANDSAT MSS. *Photogrammetric Engineering and Remote Sensing*, **49**, pp. 1303–1314.

PILON, P.G., HOWARTH, P.J., BULLOCK, R.A. and ADENIYI, P.O., 1988, An enhanced classification approach to change detection in semi-arid environments. *Photogrammetric Engineering and Remote Sensing*, **54**, pp. 1709–1716.

RUNNING, S.W., PETERSON, P.L., SPANNER, M.A. and TEUBLER, K.B., 1986, Remote sensing of coniferous leaf area. *Ecology*, **67**, pp. 273–276.

SINGH, A., 1986, Change detection in the tropical forest environment of northeastern India using Landsat. In *Remote Sensing and Tropical Land Management*, M.J. Eden and J.T. Parry (Eds) (New York, NY: John Wiley and Sons), pp. 237–254.

SINGH, A., 1989, Digital change detection techniques using remotely sensed data. *International Journal of Remote Sensing*, **10**, pp. 989–1003.

SOHL, T.L., 1999, Change analysis in the United Arab Emirates: an investigation of techniques. *Photogrammetric Engineering and Remote Sensing*, **65**, pp. 475–484.

TAPPAN, G., TYLER, D., WEHDE, M. and MOORE, D., 1992, Monitoring rangeland dynamics in Senegal with advanced very high resolution radiometer data. *Geocarto International*, **1**, pp. 87–98.

TUCKER, C.J., 1979, Red and photographic infrared linear combinations for monitoring vegetation. *Remote Sensing of Environment*, **8**, pp. 127–150.

WEISMILLER, R.A., KRISTOF, S.Y., SCHOLZ, D.K., ANUTA, P.E. and MOMIN, S.A., 1977, Change detection in coastal zone environments. *Photogrammetric Engineering and Remote Sensing*, **43**, pp. 1533–1539.

WILLIAM, E.R., WILLIAM, B.M. and TURNER, B.L., II., 1994, Modelling land use and land cover as part of global environment change. *Climatic Change*, **28**, pp. 45–64.